Final Draft
of the original manuscript:

Lozano, G.A.; Na Ranong, C.; Bellosta von Colbe, J.M.; Bormann, R.; Fieg, G.; Hapke, J.; Dornheim, M.**:**

Empirical kinetic model of sodium alanate reacting system (I). Hydrogen absorption

In: International Journal of Hydrogen Energy (2010) Elsevier

DOI: 10.1016/j.ijhydene.2010.04.080

Empirical kinetic model of sodium alanate reacting system (I). Hydrogen absorption

Gustavo A. Lozano[a,*], Chakkrit Na Ranong[b], Jose M. Bellosta von Colbe[a], Rüdiger Bormann[a], Georg Fieg[b], Jobst Hapke[b], Martin Dornheim[a]

[a] Institute of Materials Research, GKSS Research Centre Geesthacht, D-21502 Geesthacht, Germany

[b] Institute of Process and Plant Engineering, Hamburg University of Technology, D-21073 Hamburg, Germany

Abstract

Hydrogen storage systems based on metal hydrides require appropriate quantitative kinetic description for simulations and designs, in particular for the crucial absorption process. This investigation proposes an empirical kinetic model for the hydrogen absorption of sodium alanate material doped with aluminium-reduced $TiCl_4$, produced in kg-scale. The model is based on kinetic data obtained by volumetric titration measurements performed on each of the two absorption steps of sodium alanate, within a range of experimental conditions varying from 10 bar to 110 bar and from 100 °C to 180 °C. It is shown that each step is best described by the JMA model with $n = 1.33$. The kinetic equations are implemented in a mass balance and used to predict the reaction rate of the two steps of hydrogen absorption. Even when they proceed simultaneously, the predictions agree well with experimental results. The second paper of this investigation presents the results for the kinetic model of the corresponding hydrogen desorption.

1. Introduction

* Corresponding author Tel.: +49 41 5287 2643; fax: +49 41 5287 2625. Email address: gustavo.lozano@gkss.de (Gustavo A. Lozano)

Hydrogen is a very promising energy carrier for a comprehensive clean-energy concept in mobile applications. Regarding its use as fuel for the zero-emission vehicle, one main challenge is its storage. Hydrogen storage systems should fulfil the demands for automotive applications, i.e. high gravimetric and volumetric capacities, fast charging and discharging rates at moderate operating conditions, and high safety levels [1]. Metal hydrides offer a safe alternative to hydrogen storage in compressed or liquid form and have higher storage capacity by volume. Sodium alanate, $NaAlH_4$, when compared to classical room temperature hydrides, offers a suitable compromise with relatively large gravimetric storage capacity at rather moderate temperatures. Bogdanovic and Schwickardi [2] showed that hydrogen can be reversibly stored in and released from sodium alanate if doped with titanium compounds. $NaAlH_4$ is reversibly formed in a two-step reaction from NaH and Al within the technically favourable range of up to 125 °C, as shown in Eq.1 and 2. It has a theoretical gravimetric hydrogen storage capacity of 5.6 wt% based on the absorbed material, or 5.9 wt% if based on the desorbed material.

$$3NaH + Al + 1.5H_2 \leftrightarrow Na_3AlH_6 \quad (\Delta H_R = -47\ \mathrm{kJ/mol\ H_2}) \tag{1}$$

$$Na_3AlH_6 + 2Al + 3H_2 \leftrightarrow 3NaAlH_4 \quad (\Delta H_R = -37\ \mathrm{kJ/mol\ H_2}) \tag{2}$$

Looking towards practical applications, hydrogen storage systems based on metal hydrides require appropriate quantitative kinetic description for simulations, designs and evaluations. The kinetic equations must consider the rate of reaction as a function of composition, temperature, and applied hydrogen pressure. They can be used to evaluate the performance of the reactions and predict optimal operating conditions, e.g. finding the temperature with fastest kinetics for a given level of hydrogen pressure during an isothermal absorption. The present investigation aims to develop an empirical kinetic model for hydrogen absorption and desorption of sodium alanate. The material is produced in kg-scale, starting from a mixture NaH and Al doped with aluminium-reduced $TiCl_4$ [3]. This first paper of a two-part series presents the results for the model of hydrogen absorption. A second paper will present the results for hydrogen desorption.

Previous kinetic models of the absorption of sodium alanate-based material are derived from experiments in which thermodynamic conditions for both absorption steps are possible [4, 5]. However, they assumed that the second step of hydrogenation occurs only after completion of the first

step. Unlike these previous treatments, this investigation is based on the study of the individual absorption steps (as done similarly in [6]). To support the model, experiments were performed with conditions varying in the broadest interval of applied pressures and temperatures reported, from 10 bar up to 110 bar and from 100 °C to 180 °C. In addition, a new approach is proposed for the mass balance of the reactions: one in which the material is described as a mixture composed of different types of reacting materials. This avoids the use of correction terms for the experimental capacities. The mass balance is also validated with experiments in which both absorption steps can occur simultaneously. This kinetic model will be implemented in numerical simulations of hydrogen storage systems based on sodium alanate.

2. Kinetic equations

The reacting system is modelled as two consecutive absorption steps and only their net rate of reaction is considered. Equations 3 and 4 define the stoichiometry of the first and second absorption steps, respectively. Equation 3 includes the additional aluminium and hydrogen required for the second absorption step, Eq. 4.

$$3NaH + 3Al + 4.5H_2 \rightarrow Na_3AlH_6 + 2Al + 3H_2 \quad (3)$$

$$Na_3AlH_6 + 2Al + 3H_2 \rightarrow 3NaAlH_4 \quad (4)$$

Three mixtures of defined composition are used to describe the reacting system (Tang et al. [5] proposed a similar definition)

$$S_I = 3NaH + 3Al + 4.5H_2 \quad (5)$$

$$S_{II} = Na_3AlH_6 + 2Al + 3H_2 \quad (6)$$

$$S_{III} = 3NaAlH_4 \quad (7)$$

Thus, Eq. 3 corresponds to

$$S_I \rightarrow S_{II} \quad (8)$$

and Eq. 4 to

$$S_{II} \rightarrow S_{III} \quad (9)$$

The transformed fraction α will be used to follow the progress of the absorption steps and is individually considered for each step. It corresponds, among other possible relations, to the ratio of the mass of hydrogen that has been absorbed, m_{H_2}, to the maximal mass of hydrogen that can be absorbed, $m_{H_2,\max}$, Eq. 10. Equations 11 and 12 present an equivalent definition for each absorption step in terms of the masses of the mixtures of defined composition.

$$\alpha = \frac{m_{\mathrm{H_2}}}{m_{\mathrm{H_2,max}}} \tag{10}$$

$$\alpha_{\mathrm{S_I \rightarrow S_{II}}} = \frac{m_{\mathrm{S_{II}}}}{m_{\mathrm{S_I}} + m_{\mathrm{S_{II}}}} \tag{11}$$

$$\alpha_{\mathrm{S_{II} \rightarrow S_{III}}} = \frac{m_{\mathrm{S_{III}}}}{m_{\mathrm{S_{II}}} + m_{\mathrm{S_{III}}}} \tag{12}$$

The net rate of reaction of each absorption step is defined in terms of the transformed fraction:

$$\frac{d\alpha}{dt} = k(T, p)g(\alpha) \tag{13}$$

The underlying kinetic processes of the absorption, and specially the rate-limiting process, determine the net rate of reaction and consequently the function $g(\alpha)$. In this investigation the function $g(\alpha)$ is empirically determined by comparing the transformed fraction during the experiments with the value predicted by the integrated equation of different kinetic models, Table 1. The model equation with best-fit results defines the most appropriate function $g(\alpha)$. Rudman [7] and Barkhordarian et al. [8] discuss a detailed explanation about the applied models and the phenomenology behind them.

Table 1. Kinetic models used for fitting the function $g(\alpha)$ to experimental absorption data (see Eq. 13)

Model (and possible mechanism)	$g(\alpha)$	Integrated equation
Surface controlled	1	$\alpha = kt$

Johnson-Mehl-Avrami (JMA) general equation	$n(1-\alpha)\{\ln[1/(1-\alpha)]\}^{(n-1)/n}$	$[-\ln(1-\alpha)]^{1/n} = kt$
JMA, $n = 3$ (e.g. three-dimensional growth of existing nuclei with constant interface velocity)	$3(1-\alpha)\{\ln[1/(1-\alpha)]\}^{2/3}$	$[-\ln(1-\alpha)]^{1/3} = kt$
JMA, $n = 2$ (e.g. two-dimensional growth of existing nuclei with constant interface velocity)	$2(1-\alpha)\{\ln[1/(1-\alpha)]\}^{1/2}$	$[-\ln(1-\alpha)]^{1/2} = kt$
JMA, $n = 1$ (e.g. one-dimensional growth of existing nuclei with constant interface velocity)	$(1-\alpha)$	$-\ln(1-\alpha) = kt$
Contracting Volume (CV) (e.g. contracting volume, three-dimensional growth with constant interface velocity)	$3(1-\alpha)^{2/3}$	$1-(1-\alpha)^{1/3} = kt$
CV (e.g. contracting volume, two-dimensional growth with constant interface velocity)	$2(1-\alpha)^{1/2}$	$1-(1-\alpha)^{1/2} = kt$
CV (e.g. contracting volume, three dimensional growth diffusion controlled with decreasing interface velocity)	$3/2\left[(1-\alpha)^{-1/3}-1\right]^{-1}$	$1-(2\alpha/3)-(1-\alpha)^{2/3} = kt$

The rate constant k in Eq. 13 is a function of the temperature and the applied hydrogen pressure:

$$k(T,p) = \left(Ae^{-\frac{E_a}{RT}}\right) f(p, p_{eq}) \tag{14}$$

The first factor of Eq. 14 is the Arrhenius formula, while the second factor reflects the influence of the equilibrium and applied pressure on the net rate of reaction. This influence is a consequence of the reversible character of the reaction. The factor $f(p, p_{eq})$ acts as the driving force of the absorption, which depends on the deviation of p from p_{eq}. In this work, the factor $f(p, p_{eq})$ is defined by trying different functions and selecting the one that best fits the experimental data. Some of the considered functions are $\ln(p/p_{eq})$ (since it defines the change of free energy of the sorption

process), $(p - p_{eq})/p_{eq}$ (a first order approximation of the logarithm based on its Taylor series), and combinations of them. However, other empirical functions may be also tried for the factor $f(p, p_{eq})$. The procedure to obtain the parameters A, E_a, and the functions $g(\alpha)$ and $f(p, p_{eq})$, from experimental data is as follows:

1. The function $g(\alpha)$ is determined by fitting the experimental data to the integrated equations of the models in Table 1. The model with best-fit results defines $g(\alpha)$. The experiments must be performed isothermal and isobaric.

2. After a model has been found to define function $g(\alpha)$, the values of the rate constant k for each experiment are determined, i.e. $k(T, p)$

3. A function for the factor $f(p, p_{eq})$ is assumed. The parameters A and E_a are calculated using the experimental values of k by fitting $\ln[k/f(p, p_{eq})]$ vs. $1/T$ (see Eq. 14). In a next step, the correlation fit is evaluated and $\ln(k/\{A \cdot \exp[-Ea/(RT)]\})$ vs. $f(p, p_{eq})$ is plotted. A perfect fitting of the later relation is a line that crosses the origin and has a slope equal to 1.

4. Other functions $f(p, p_{eq})$ should be considered, and the correlation of the plots mentioned in step 3 of this procedure is compared. The function with best results is the one that best describes the kinetics.

3. Experimental procedures

3.1. Production of materials

All material for the kinetic measurements was produced in an industrial scale like milling equipment (ESM 236, Siebtechnik, Mühlheim a. d. R., Germany) and optimised towards fast kinetics [3]. The raw materials were commercial NaH (95%, Sigma Aldrich Chemie GmbH, Steinheim, Germany), aluminium (99,5%, Johnson Matthey GmbH & Co. KG, Karlsruhe, Germany), aluminium-reduced $TiCl_4$ as catalyst precursor (Fluka Chemie GmbH, Buchs, Switzerland), and carbon powder as milling agent (graphite powder, Alfa Aesar GmbH &Co. KG, Karlsruhe, Germany). All handling, including

milling, was carried out in a glove box with purified argon atmosphere. Prior to milling, NaH and aluminium were mixed in a tumbling shaker for 0.5 h in a molar ratio of 1.08 to 1 according to the reaction:

$$\begin{aligned} &1.08\,\mathrm{NaH} + \mathrm{Al} + 0.02(\mathrm{TiCl_3} + \tfrac{1}{3}\mathrm{AlCl_3}) \\ &\rightarrow \mathrm{NaH} + 1.0067\mathrm{Al} + 0.08\mathrm{NaCl} + 0.02\mathrm{Ti} + 0.04\mathrm{H_2} \end{aligned} \quad (15)$$

This reaction is expected to occur during milling. Milling was carried out in a modified vibratory tube mill, using 30-mm hardened balls at a rotational speed of 1000 rpm and a ball-to-powder ratio (BPR) of 140:1. Total milling time was 6.5 h.

3.2. Kinetic measurements

Sorption kinetics was characterized using a Sieverts' type apparatus (HERA, Quebec, Canada) that works based on a pressure-volumetric method combined with differential-pressure measurements [9]. A cylindrical sample cell of 2 mm diameter was utilized. During all the experiments the temperature on the outer wall of the cell was measured. The milled material was filled into the cells inside an argon glove box. The cell was loaded with the milled material up to its top and immediately weighed afterwards (with a mg precision scale). The mass of material in the cell was between 40 mg and 50 mg.

To study the reaction kinetics of each absorption step individually, pressure-temperature (p-T) pairs for the initial and final states were chosen such that only one reaction step took place. The measurements were performed with both initial and final states at the same temperature. At time $t = 0$ of the experiment the initial pressure was raised stepwise to the pressure of the final state. Figure 1 shows the thermodynamic stable states of the reacting system according to p-T conditions. The equilibrium lines are calculated using the van 't Hoff equation and the parameters determined in [10] for the sodium alanate reacting system. Equations 16 and 17 are the van 't Hoff equilibrium lines for the first and second absorption steps, respectively.

$$\ln\left(\frac{p_{eq,\mathrm{S_I}\leftrightarrow\mathrm{S_{II}}}}{1\,\mathrm{bar}}\right) = \frac{\Delta \mathrm{H}_{\mathrm{R},\mathrm{S_I}\leftrightarrow\mathrm{S_{II}}}}{RT} - \frac{\Delta \mathrm{S}_{\mathrm{R},\mathrm{S_I}\leftrightarrow\mathrm{S_{II}}}}{R} = -\frac{47\,\mathrm{kJ\,mol\,H_2^{-1}}}{RT} + \frac{126\,\mathrm{J\,mol\,H_2^{-1}\,K^{-1}}}{R} \quad (16)$$

$$\ln\left(\frac{p_{eq,S_{II}\leftrightarrow S_{III}}}{1\,\text{bar}}\right)=\frac{\Delta H_{R,S_{II}\leftrightarrow S_{III}}}{RT}-\frac{\Delta S_{R,S_{II}\leftrightarrow S_{III}}}{R}=-\frac{37\,\text{kJ mol H}_2^{-1}}{RT}+\frac{122\,\text{J mol H}_2^{-1}\,\text{K}^{-1}}{R} \quad (17)$$

Table 2 summarizes initial and final conditions used to study each absorption step. All the experimental results for the kinetic analysis correspond to measurements of material that had been absorbed and desorbed at least 3 times, after which the material shows reproducible kinetics with respect to cycling.

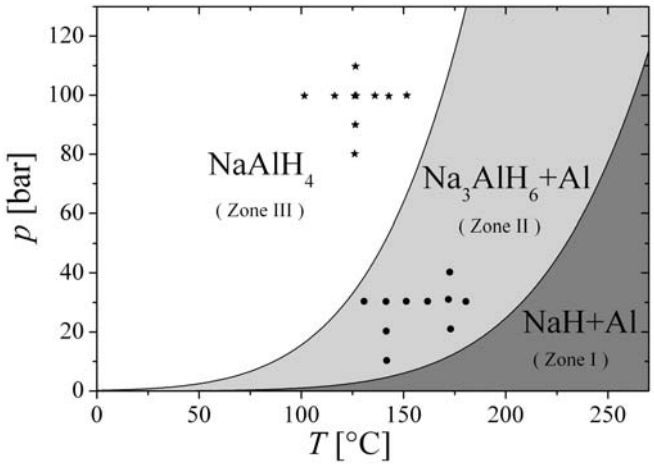

Figure 1. p-T diagram presenting the most stable state of the sodium alanate reacting system under H_2 pressure. At p-T conditions inside zones I, II and III, NaH+Al , Na_3AlH_6+Al, and $NaAlH_4$, respectively, are the most stable solid states. The circles (•) and the stars (★) correspond to p-T conditions for experiments for the first and second absorption steps, respectively

Table 2. Location of the initial and final states for the absorption experiments according to the zones on Fig. 1

Absorption step	Reaction	Initial State	Final State
First	$3NaH + 3Al + 4.5H_2 \rightarrow Na_3AlH_6 + 2Al + 3H_2$	Zone I	Zone II
Second	$Na_3AlH_6 + 2Al + 3H_2 \rightarrow 3NaAlH_4$	Zone II	Zone III

4. Results and Discussion

4.1 Isobaric and isothermal conditions during measurements

Both pressure and temperature during kinetic measurements must remain constant according to the quantitative analysis presented. If neither this issue nor the effects of the heat flow and mass flow are taken into account, kinetic analyses could be invalid and lead to wrong conclusions about the intrinsic kinetics [7].

The Sieverts' type apparatus uses the change of the hydrogen pressure to follow the extent of the sorption reactions. Therefore, isobaric experiments are impossible to perform with this equipment [9]. To minimize this pressure change and maintain good resolution in the results, the apparatus worked with high gaseous reference volumes. The highest pressure change during the absorption measurements was -0.25 bar, while the pressure level is between 10 and 100 bar. The pressure used in the analysis was the arithmetic mean during each experiment.

Because of the high enthalpy of reaction of the investigated system, isothermal conditions cannot be perfectly maintained. It was shown that sorptions in even small cells lead to significant changes of temperature of the reacting material during the process [11]. To minimize the temperature increase or decrease, the kinetic measurements were done in a 2-mm cell, which maintains almost isothermal behaviour: finite element simulations of the sorption process in the 2-mm cell demonstrated that the temperature increase of the material is lower than 1 K under the conditions and rates obtained in the experiments. The geometry of the cell is presented elsewhere [11]. Figure 2 shows the results of the simulation of a hydrogenation of totally desorbed material at 100 bar and 125 °C. Under these conditions, the process has a high rate of reaction and, therefore, high rate of heat release and temperature increase are expected. The simulation of the bed of material applied the standard equation of heat conduction with a heat source, Eq. 18. The heat source is calculated from the experimental hydrogen sorption rate per mass of reacting material, the bulk density and the enthalpy of reaction derived from PcT-measurements (see Eq. 16.)

$$c_{p,b}\rho_b \frac{\partial T}{\partial t} = \lambda_b \nabla^2 T - r' \rho_b \Delta \mathrm{H_R} \tag{18}$$

The heat conduction through the cell wall was simulated with the equation of heat conduction without any heat source term. The surface temperature of the cell wall had a constant temperature of 125 °C as

it was measured during the experiments. The properties of the bed of material are as follows: density: 0.55 g ml^{-1} (experimental), heat capacity: 1075 J kg^{-1} K^{-1} [12], and thermal conductivity: 0.5 W m^{-1} K^{-1} [11]. The cell walls are made of stainless steel with a density of 7.9 g ml^{-1}, a heat capacity of 500 J kg^{-1} K^{-1}, and a thermal conductivity of 15 W m^{-1} K^{-1} [13]. The sensible heat of the gaseous phase and the kinetic energy of the incoming hydrogen were neglected. Franzen [6] presents a detailed explanation of finite element simulations of hydrogen absorption process with sodium alanate in similar geometries.

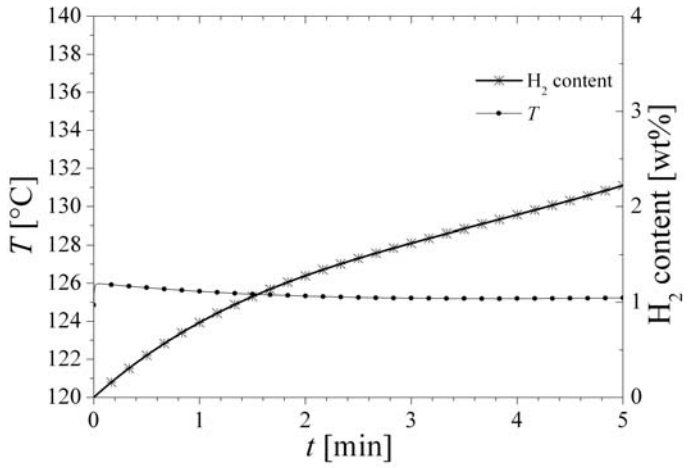

Figure 2. Simulated temperature development inside the 2-mm cell during an experimental absorption at 100 bar. Initial temperature is 125 °C. T is the temperature in the centre of the bed of reacting material.

4.2 Hydrogen absorption of NaH+Al to form Na_3AlH_6: $S_I \rightarrow S_{II}$

The absorption experiments were done at p-T pairs with starting state within zone I and final state within zone II according to Fig. 1. To guarantee the starting state of the material within zone I, desorptions with final conditions within zone I were done until the material was fully desorbed. Afterwards, the material was put under vacuum at 180 °C for one hour. In this investigation, the transformed fraction $\alpha_{S_I \rightarrow S_{II}}$ considers only the active absorbing material and it is referred to the total hydrogen absorbed in each experiment after completion and therefore goes always from 0 to 1. The

experimental hydrogen capacity of the absorption experiments was 1.6 wt%, which corresponds to 94% of the theoretical capacity of 1.7 wt% of the first absorption step for the mixture of this investigation. The capacities are calculated based on the desorbed material including all inert species (catalysts and additional carbon).

The effect of temperature on the rate of reaction at constant pressure is shown in Fig. 3, which presents hydrogen absorption curves at 30 bar and temperatures between 130 °C and 180 °C. Clearly, the rate of absorption increased from 130 °C to 170 °C. At 180 °C, however, only a slight increase in the reaction rate is observed as compared to 170 °C. The equilibrium temperature at 30 bar for the first absorption step corresponds to 208 °C according to Eq. 16 (see also Fig. 1). As the temperature for the absorption experiments gets close to this equilibrium value, the rate of reaction should decrease and therefore there is a temperature before equilibrium that has the maximum rate of absorption. According to the results at 30 bar, the temperature of the maximum rate of absorption should be in the vicinity of 170 °C and 180 °C. This value will be compared in this subsection by means of the derived analytical expression of the kinetics model.

Absorption curves at 140 °C are shown in Fig. 4 for pressures from 10 bar to 30 bar. At 10 bar it is already possible to reach 40% of the hydrogen capacity of the first step of absorption after only 20 minutes. After 2 hours, the absorption is almost complete (not shown on the figure). By increasing the pressure at the same temperature, the rate of absorption gets significantly faster. At 20 bar, the time to absorb 90% of the hydrogen capacity is reduced to less than 15 minutes, and at 30 bar it is reduced to 7 minutes.

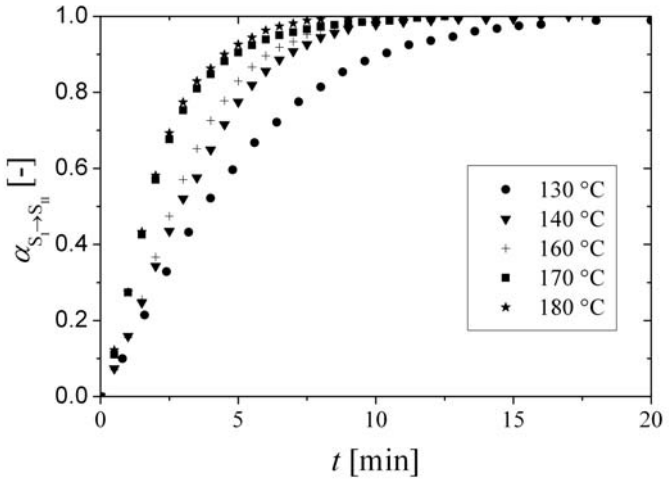

Figure 3. Hydrogen absorptions of NaH+Al at 30 bar and temperatures between 130 °C and 180 °C. The transformed fraction is normalized to the total mass of hydrogen absorbed in each experiment after completion.

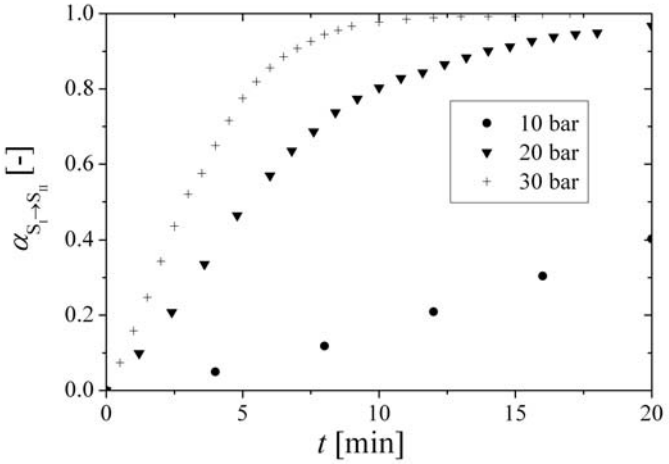

Figure 4. Hydrogen absorptions of NaH+Al at 140 °C and pressures between 10 bar and 30 bar.

The rate of the first absorption step was fitted by applying the procedure explained in Section 2. The rate of absorption is best described by the JMA model with n=1.33.

$$\frac{d\alpha_{S_I \to S_{II}}}{dt} = 1.33 k_{S_I \to S_{II}} \left(1 - \alpha_{S_I \to S_{II}}\right) \left\{ \ln\left(\frac{1}{1 - \alpha_{S_I \to S_{II}}} \right) \right\}^{0.25} \tag{19}$$

Following the procedure, the constant $k_{S_I \rightarrow S_{II}}$ is determined for each experiment. Based on these values, further fitting of Eq. 14 led to the function

$$f_{S_I \rightarrow S_{II}}(p, p_{eq}) = \left(p - p_{eq}\right) / p_{eq} \tag{20}$$

with Arrhenius parameters A=2.28 10^8 s^{-1} and E_a=91.7 kJ mol^{-1}. Figure 5 shows the results of the fitting of the experimental data with these function and parameters.

The exponent value n=1.33 may suggest spatial or temporal superposition of transformation mechanisms. For instance, it could be superposition of two and three dimensional growth of constant number of nuclei at a diffusion controlled transformation. The JMA equation with exponent value n=1.33 for this absorption step is similar to the kinetic model in [6, 14], which reported an empirical equation for this absorption step using the JMA equation with n =1.4 and n=1. Kircher and Fichtner [15] applied also the JMA equation to the first absorption step, reporting values of n varying between 0.7 to 0.8 depending on the sample preparation method.

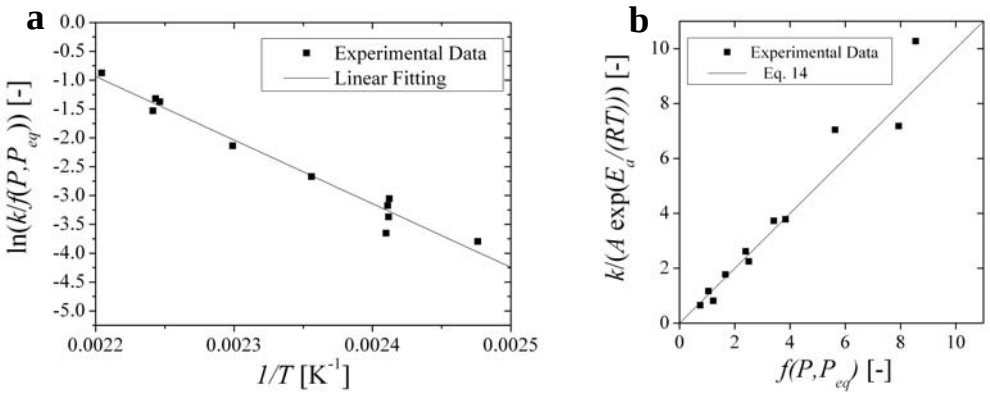

Figure 5. Kinetic fitting of the absorption of NaH+Al to Na_3AlH_6. Equation 14 defines the fitting relation. The parameters A and E_a in the right diagram (b) come from the fitting in the left diagram (a) (A=2.28 10^8 s^{-1} and E_a=91.7 kJ mol^{-1}).

To complement the analysis, the rate constant $k_{S_I \rightarrow S_{II}}$ is calculated and extrapolated for several p-T conditions by using Eq. 14 and parameters of the fitting, and presented in Fig. 6. At conditions with pressures lower than the equilibrium pressure of the first absorption step, NaH+Al should not absorb

hydrogen and therefore the rate constant for the absorption is set to 0. The constant rate lines of the contour demonstrate that by changing conditions it is possible to have the same rate of reaction at different temperatures by decreasing the pressure, e.g. the absorption at 120 °C and 40 bar and at 154 °C and 20 bar. The contour also indicates that for every pressure there is a maximum value of the rate of reaction and there are also two temperatures that have the same rate of reaction. One of them is lower than the temperature of the maximum rate of reaction. The second one is higher but still lower than the corresponding equilibrium temperature. The temperature of maximum rate of reaction can be analytically deduced by combining Eqs. 14 and 20:

$$T_{Opt} = \frac{-\Delta \mathrm{H_R}}{R\left[\ln\left(\frac{E_a}{E_a + \Delta \mathrm{H_R}}\right) - \ln\left(\frac{p}{1\ \mathrm{bar}}\right)\right] - \Delta \mathrm{S_R}} \tag{21}$$

Equation 21 has utility when defining optimal process conditions for hydrogen absorptions. The dotted line on Fig. 6 shows the calculated points of maximum rate of reaction for every pressure. At 30 bar, the optimal temperature corresponds to 180 °C and confirms the experimental results in Fig. 3. Also, because the contour lines are becoming vertical, it is concluded that the effect of pressure on the rate of reaction is low when p-T conditions are far from the optimal conditions line. At conditions close to this line, however, the contour lines become horizontal and the effect of the pressure on the rate of reaction is thus the highest. When applying the same analysis to the effect of the temperature on the rate of reaction, it is concluded that far away from the optimal conditions line, the effect of temperature is great, while at the optimal conditions line its effect is the least.

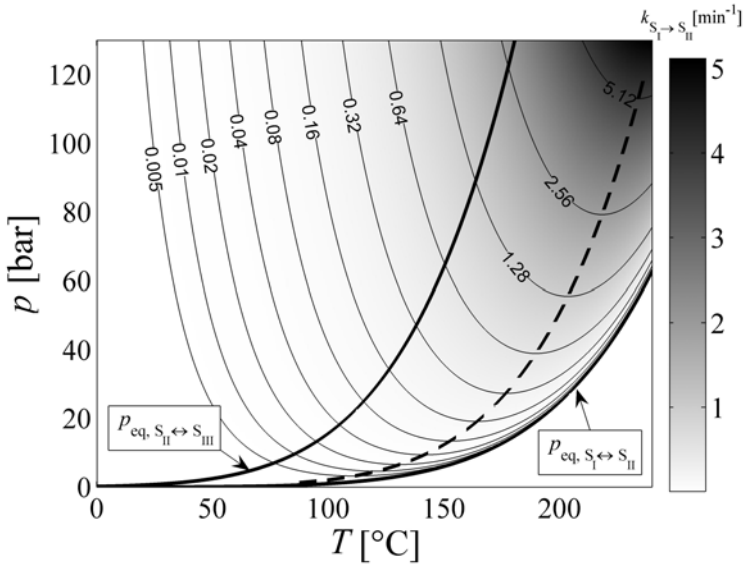

Figure 6. Calculated values of the rate constant $k_{S_I \rightarrow S_{II}}$ as a function of pressure and temperature. The lines are contour lines of values having the same rate constant. The dotted line represents the calculated points of maximum rate of reaction for every pressure.

4.3 Hydrogen absorption of Na_3AlH_6+Al to form $NaAlH_4$: $S_{II} \rightarrow S_{III}$

The experiments for this absorption step had p-T starting state within zone II and final state within zone III according to Fig. 1. Desorptions with final conditions within zone II guaranteed the starting state of the material. They last until the expected hydrogen capacity was reached. As done for the first absorption step, the reported transformed fraction $\alpha_{S_{II} \rightarrow S_{III}}$ considers only the active absorbing material and therefore goes always from 0 to 1. The absorption experiments yielded a hydrogen capacity of 2.3 wt%, which corresponds to 68% of the theoretical capacity of 3.4 wt% of the second absorption step. The reduction of the capacity is explained by the inhomogeneous distribution of the reacting solid phases [4, 16]. The inhomogeneous distribution of NaH and Al for the formation of Na_3AlH_6 during the hydrogen absorption, Eq. 1, leads to the first inefficiency of the process. Later, during the hydrogenation of Na_3AlH_6+Al, Eq. 2, some Na_3AlH_6 does not react further with Al and acts as inert species for this reaction. If an efficiency of 94% for the first absorption step is considered, the efficiency of the second absorption step becomes 72%. The aluminium in excess for the first absorption step, which is actually required for the second absorption step, explains the higher efficiency of this first step.

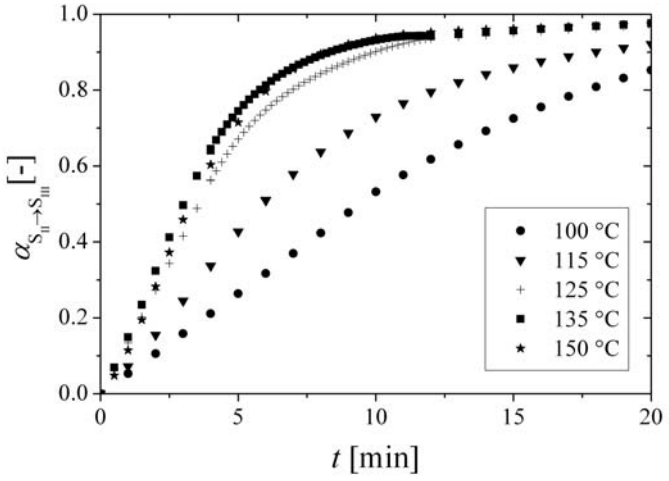

Figure 7. Hydrogen absorptions of Na_3AlH_6+Al at 100 bar and temperatures between 100 °C and 150 °C. The transformed fraction is normalized to the total mass of hydrogen absorbed in each experiment after completion.

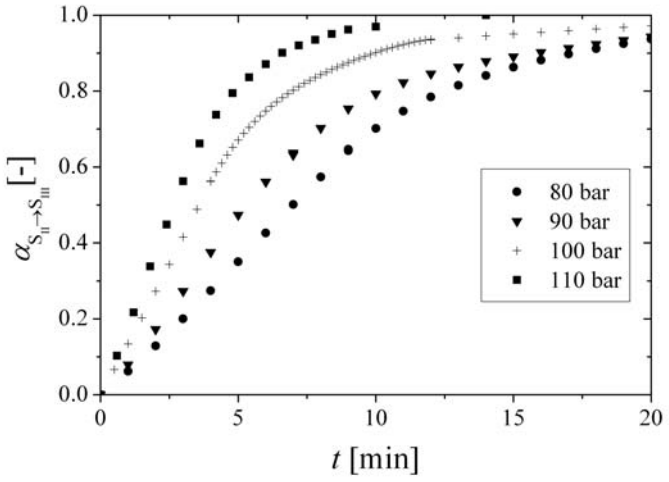

Figure 8. Hydrogen absorptions of Na_3AlH_6+Al at 125 °C and pressures between 80 bar and 110 bar.

Figure 7 shows the effect of temperature on the rate of reaction at constant pressure for hydrogen absorptions at 100 bar and temperatures between 100 °C and 150 °C. The behaviour is similar to the first absorption step: the rate of absorption increased from 100 °C to 135° C, but at 150 °C, however,

there is a slight decrease in the reaction rate. The equilibrium temperature for this absorption step is 169 °C at 100 bar according to Eq. 17. At 100 bar, the maximum rate of absorption should be close to 135 °C and 150 °C.

Figure 8 shows absorption results at 125 °C and pressures in the range of 80 bar to 110 bar. The effect of pressure is clear, improving the rate of reaction by increasing the driving force. At 125 °C and 110 bar it is possible to absorb 90% of the hydrogen capacity within 7 minutes.

As for the first absorption step, the JMA model with n =1.33 describes the rate of the second absorption step.

$$\frac{d\alpha_{S_{II}\rightarrow S_{III}}}{dt} = 1.33 k_{S_{II}\rightarrow S_{III}} \left(1-\alpha_{S_{II}\rightarrow S_{III}}\right) \left\{ \ln\left(\frac{1}{1-\alpha_{S_{II}\rightarrow S_{III}}} \right) \right\}^{0.25} \tag{22}$$

The fitting procedure of the constant $k_{S_{II}\rightarrow S_{III}}$ of each experiment led to the function

$$f_{S_{II}\rightarrow S_{III}}(p, p_{eq}) = \left(p - p_{eq}\right) / p_{eq} \tag{23}$$

The fitted Arrhenius parameters are A=1.52 10^9 s^{-1} and E_a =91.5 kJ mol^{-1}. Franzen and Na Ranong et al. [6, 14] also found that the first and second absorption steps have the same JMA order (n =1.4 and n =1). Kircher and Fichtner [15] reported a JMA order n of 1.1 and 1.4 for this second absorption step. The p-T diagram on Fig. 9 shows the calculated and extrapolated values of the rate constant $k_{S_{II}\rightarrow S_{III}}$.

When the applied pressure is lower than the equilibrium pressure of the second absorption step, the rate constant is set to 0. Moreover, if the pressure is even lower than the equilibrium pressure of the first absorption step, Na_3AlH_6 should desorb hydrogen and form NaH+Al. These conditions are, however, not of interest for the present analysis. The zone of conditions for the absorption of the second step is smaller than for the first one and therefore the conditions of the second step of reaction will have stronger influence on the operation when it is desired to work with both steps simultaneously. Compared to the first absorption step, the second step is slower under the same applied conditions. The contour lines of constant reaction rate illustrate the possibility to obtain the same rate of reaction at different temperatures and pressures e.g. the absorption at 120 °C and 100 bar and at 155 °C and 90 bar. The dotted line on Fig. 9, plotted based on Eq. 21, shows the points of

maximum rate of reaction for every pressure. At 100 bar the optimum temperature corresponds to 147 °C, which reflects the result obtained in the experimental measurements given in Fig. 7.

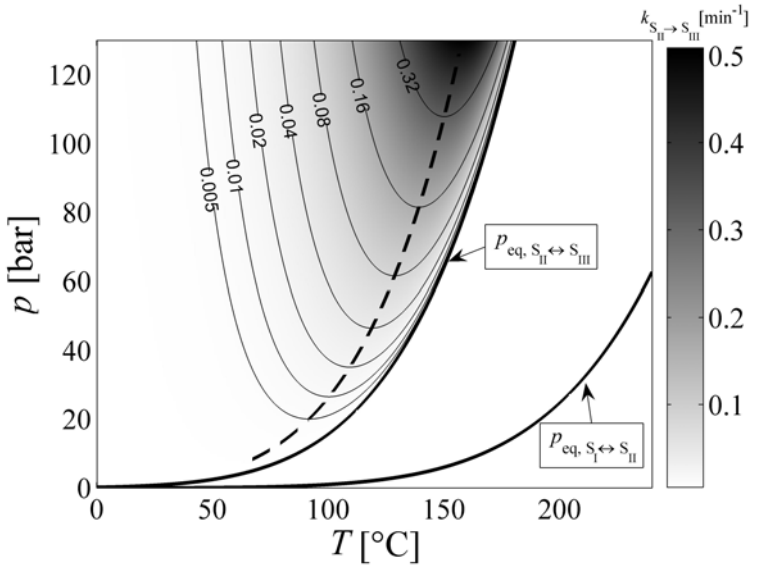

Figure 9. Calculated values of the rate constant $k_{S_{II}\rightarrow S_{III}}$ as a function of pressure and temperature. The lines are contour lines of values having the same rate constant. The dotted line represents the calculated points of maximum rate of reaction for every pressure.

4.4 Empirical kinetic model and validation

The combination of both absorption steps as a model of two consecutive reactions describes the process when the steps can proceed one after the other and simultaneously because of thermodynamic conditions. This is the case when changing conditions from zone I to zone III of Fig. 1. As soon as NaH+Al is hydrogenated to Na_3AlH_6, Na_3AlH_6+Al can react further with hydrogen to form $NaAlH_4$. The combination of Eqs. 8 and 9 defines the reacting system:

$$S_I \xrightarrow{r_{a1}} S_{II} \xrightarrow{r_{a2}} S_{III} \tag{24}$$

The mass balance of the two consecutive reactions is summarized in the following equations:

$$\frac{dm_{S_I}}{dt} = -r_{a1} \tag{25}$$

$$\frac{dm_{S_{II}}}{dt} = r_{a1} - r_{a2} \tag{26}$$

$$\frac{dm_{S_{III}}}{dt} = r_{a2} \tag{27}$$

Thus, the use of this mass balance avoids the approximation of considering that the second absorption starts only until the first one is completed or the use of empirical correlations for the mass balance. The instantaneous rates of reaction in terms of masses are derived based on the kinetic equations when each absorption step independently occurs, Eqs. 19 and 22. Under this condition the total mass of the reacting system $m_{S_I} + m_{S_{II}}$ and $m_{S_{II}} + m_{S_{III}}$ is constant during the first and second absorption steps, respectively.

From Eqs. 10-12, 19 and 25-27, the instantaneous rate of the first absorption step in term of masses becomes

$$r_{a1} = 1.33 k_{S_I \rightarrow S_{II}} m_{S_I} \left\{ \ln\left(\frac{m_{S_I} + m_{S_{II}}}{m_{S_I}} \right) \right\}^{0.25} \tag{28}$$

and correspondingly the instantaneous rate of the second absorption step:

$$r_{a2} = 1.33 k_{S_{II} \rightarrow S_{III}} m_{S_{II}} \left\{ \ln\left(\frac{m_{S_{II}} + m_{S_{III}}}{m_{S_{II}}} \right) \right\}^{0.25} \tag{29}$$

Finally, the model considers that a mixture of three types of material composes the reacting system:

1. Material that can form NaH+Al, Na_3AlH_6 and $NaAlH_4$.

2. Material that can form NaH+Al and Na_3AlH_6 but not $NaAlH_4$. (inert material for the second absorption step)

3. Material that does not react at all (inert material for both absorption steps)

This new approach for the material balance eliminates the use of artificial terms in the kinetic equations to limit the capacities to the experimentally obtained ones as it is done in other kinetic models for sodium alanate [4-6, 14]. The ratios of these materials are based on the stoichiometry of the system and on the achieved experimental hydrogen capacities. Table 3 shows the mass composition of the material used in this investigation. These mass fractions are calculated based on the masses of the initial raw materials, the measured experimental hydrogen capacities and the stoichiometry of the system (Eqs. 1 and 2).

Table 3. Mass composition of the different type of materials according to experimental results.

Type of Material	Mass fraction in the initial mixture [-]
Active material for both absorption steps	0.58
Active material for the first absorption step only	0.23
Inert material	0.19

Figure 10 presents some calculated absorption curves based on the proposed kinetic model under various operating conditions. To validate the model, the figure also shows the respective experimental results. It can be seen from the figure that the model reflects the experimentally measured data accurately. This validation, which complements the results of the individual absorption steps presented in Sections 4.2 and 4.3, ensures reliability of the presented fitting procedure and the empirical kinetic model. The model can be numerically implemented for simulations, designs and evaluations of hydrogen storage systems based on sodium alanate material as produced in this work. The proposed fitting procedure and material balance is also suitable for the development of empirical kinetic models for other metal hydride systems.

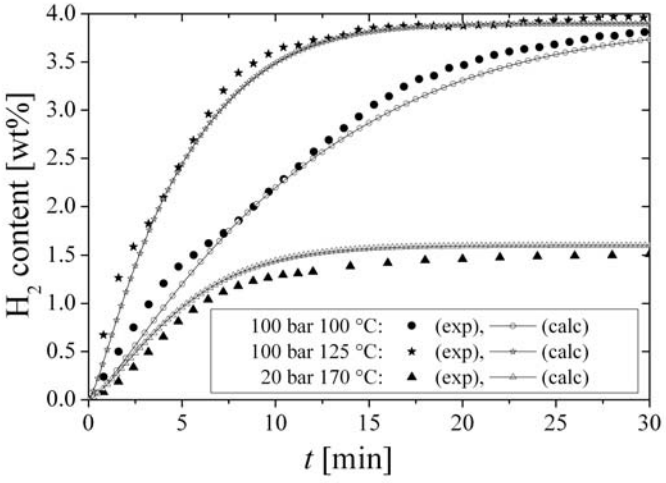

Figure 10. Experimental and calculated absorptions of totally desorbed sodium alanate material at different conditions. The calculations use the model presented in Section 4.3.

5. Conclusions

Aiming to develop a tool for evaluation, simulation and design of hydrogen storage tanks based on sodium alanate, an empirical kinetic model has been determined for the first and second absorption steps of the sodium alanate system. The material used in the kinetic investigation comes from a kg-scale production process to ensure utilization of the model for future technological systems. To support the model, kinetic measurements were performed on a broad range of p-T conditions, which were performed when the material had practically steady kinetics with respect to cycling. The implemented experimental procedure allowed the independent study of the kinetics of each absorption step. During each kinetic measurement the pressure was effectively constant, and in addition a simulation analysis verified that the experiments were isothermal in the range of ±0.5 K. The obtained kinetic equations for each absorption step take into consideration not only the effect of temperature and transformed fraction, but also the applied hydrogen pressure and the corresponding equilibrium pressure. Thus, the model allows the evaluation of the absorption reactions under technological conditions. A structured procedure for the fitting was presented and successfully applied in the results, which can be used in other systems as well.

It was found that both absorption steps fit very well the JMA model with n=1.33. The first absorption step, however, presents faster kinetics than the second step. In both steps it was shown that for a given level of pressure there is a temperature with fastest kinetics. Based on the kinetic model, an expression was derived that allows the prediction of this optimal temperature. The predicted values agree with the experimental results for both steps. For instance, the expression predicts an optimal temperature of 147°C for the formation of $NaAlH_4$ under 100 bar of hydrogen pressure.

A model of the two absorption steps as two consecutive reactions was developed and validated. A new approach for the material balance of the reactions, which categorise the material in three different types, eliminates the use of artificial terms in the kinetic equations to fit the calculated capacities to the experimental ones. The stoichiometry and the experimental hydrogen capacities define the ratios of the types of materials. The model will be implemented for numerical simulations, designs and evaluations of hydrogen storage systems based on sodium alanate.

Acknowledgments

The authors appreciate the financial support of the European Community in the frame of the Integrated Project "NESSHY—Novel Efficient Solid Storage for Hydrogen" (contract SES6-CT-2005-518271) and of the Helmholtz Initiative "FuncHy—Functional Materials for Mobile Hydrogen Storage".

Nomenclature

A	pre-exponential factor of Arrhenius formula, s^{-1}
$c_{p,b}$	heat capacity of the bed of material, J kg^{-1} K^{-1}
CV	contracting volume model
E_a	energy of activation of Arrhenius formula, J mol^{-1}
f	function of p and p_{eq} that acts as driving force for the absorption reaction, -
g	function that defines the rate of reaction, -
JMA	Johnson-Mehl-Avrami model
k	rate constant, s^{-1}
m	mass, kg
n	kinetic order of the JMA equation, -
p	pressure, bar
p_{eq}	equilibrium pressure, bar
p-T	pressure-temperature
r_{a1}	net rate of the first absorption step, g s^{-1}
r_{a2}	net rate of the second absorption step, g s^{-1}
r'	hydrogen sorption rate per mass of reacting material, mol H_2 g^{-1} s^{-1}
R	gas universal constant, 8.314 J mol^{-1} K^{-1}
S_I	mixture of 3 mol NaH, 3 mol Al, and 9/2 mol H_2
S_{II}	mixture of 1 mol Na_3AlH_6, 3 mol Al, and 3 mol H_2

S_{III} 3 mol $NaAlH_4$

t time, s

T temperature, K

T_{Opt} optimal temperature, K

Greek

α transformed fraction, -

ΔH_R enthalpy of reaction per mol of hydrogen, J mol H_2^{-1}

ΔS_R entropy of reaction per mol of hydrogen, J mol H_2^{-1} K^{-1}

λ_b effective thermal conductivity of the bed of material, W m^{-1} K^{-1}

ρ_b density of the bed of material, kg m^{-3}

References

[1] StorHy. StorHy Final Publishable Activity Report. 2008. http://www.storhy.net/pdf/StorHy_FinalPublActivityReport_FV.pdf; [viewed 02.10.2009]

[2] Bogdanovic B, Schwickardi M. Ti-doped alkali metal aluminium hydrides as potential novel reversible hydrogen storage materials. J. Alloys Compd. 1997;253-254:1-9.

[3] Eigen N, Keller C, Dornheim M, Klassen T, Bormann R. Industrial production of light metal hydrides for hydrogen storage. Scripta Mater. 2007;56:847-851.

[4] Luo W, Gross KJ. A kinetics model of hydrogen absorption and desorption in Ti-doped NaAlH4. J. Alloys Compd. 2004;385:224-231.

[5] Tang X, Mosher DA, Anton DL. Practical sorption kinetics of TiCl3 catalyzed NaAlH4. Mater. Res. Soc. Symp. Proc. 2005;Vol 884E:GG4.4.

[6] Franzen J. Modellierung und Simulation eines Wasserstoffspeichers auf der Basis von Natriumalanat. VDI-Fortschrittsberichte, 6 (583), VDI-Verlag, Düsseldorf 2009.

[7] Rudman PS. Hydriding and dehydriding kinetics. Journal of the Less Common Metals 1983;89:93-110.

[8] Barkhordarian G, Klassen T, Bormann R. Kinetic investigation of the effect of milling time on the hydrogen sorption reaction of magnesium catalyzed with different Nb2O5 contents. J. Alloys Compd. 2006;407:249-255.

[9] Schulz R, Huot J, Boily S. Equipment fo gas titration and cycling of an absorbent or adsorbent material. Can. Patent.,Ser.-Nr. 2207149. 1999.

[10] Bogdanovic B, Brand RA, Marjanovic A, Schwickardi M, Tölle J. Metal-doped sodium aluminium hydrides as potential new hydrogen storage materials. J. Alloys Compd. 2000;302:36-58.

[11] Lozano GA, Eigen N, Keller C, Dornheim M, Bormann R. Effects of heat transfer on the sorption kinetics of complex hydride reacting systems. Int. J. Hydrogen Energy 2009;34:1896-1903.

[12] Dedrick DE, Kanouff MP, Replogle BC, Gross KJ. Thermal properties characterization of sodium alanates. J. Alloys Compd. 2005;389:299-305.

[13] Davis JR, editor. Stainless steels. Materials Park, Ohio: ASM International, 1994.

[14] Na Ranong C, Höhne M, Franzen J, Hapke J, Fieg G, Dornheim M, Eigen N, Bellosta von Colbe JM, Metz O. Concept, Design and Manufacture of a Prototype Hydrogen Storage Tank Based on Sodium Alanate. Chemical Engineering & Technology 2009;32:1154-1163.

[15] Kircher O, Fichtner M. Hydrogen exchange kinetics in NaAlH4 catalyzed in different decomposition states. J. Appl. Phys. 2004;95:7748-7753.

[16] Eigen N, Gosch F, Dornheim M, Klassen T, Bormann R. Improved hydrogen sorption of sodium alanate by optimized processing. J. Alloys Compd. 2008;465:310-316.